Journal of Manufacturing Processes 83 (2022) 116–128

Contents lists available at ScienceDirect

Journal of Manufacturing Processes

journal homepage: www.elsevier.com/locate/manpro

Continuous coaxial nozzle designs for improved powder focusing in direct laser metal deposition

Theodore Gabor [a], Huitaek Yun [b], Semih Akin [a], Kyung-Han Kim [c], Jong-Kwon Park [c], Martin Byung-Guk Jun [a,*]

[a] School of Mechanical Engineernig, Purdue University, 585 Purdue Mall, West Lafayette 47907-2088, IN, USA
[b] Indiana Manufacturing Competitiveness Center (IN-MaC), Purdue University, 1105 Endeavor Drive Suite 400, West Lafayette 47906, IN, USA
[c] Advanced Manufacturing Systems Research Division, Korean Institute of Machinery and Materials, Yuseong-Gu, Daejeon 34103, South Korea

ARTICLE INFO

Keywords:
Additive manufacturing (AM)
Direct laser deposition (DLMD)
Direct
Metal deposition (DMD)
Direct laser metal deposition (DLMD)
Metal
Additive manufacturing
Nozzle design

ABSTRACT

Direct Laser Metal Deposition (DLMD) is a type of Additive Manufacturing (AM) that deposits blown metallic powders from a nozzle onto a substrate. These powders are then simultaneously fused together by a high powered (0.1–1 *kW*, often ND:YAG) laser to form a deposited layer. Out of the various nozzle designs Continuous Coaxial nozzles provide the most even spray profile due to their annular profile. This is at the cost of a reduction in spray focusing. In this paper, the authors use full factorial analysis of simulated gas-powder nozzle flows to determine the impact of inlet pressure (1–10 *kPa*), powder inlet angle (0° – 25°), powder inlet offset (0–10 *mm* offset from the centerline), and internal groove shape (no grooves, straight grooves, tapered grooves) on nozzle focusing and powder velocity. It was determined that 1 mm wide straight grooves provided the best focusing, with powder concentrations reaching from 0.3 to 0.45 kg/m^3 and particle cloud diameters reaching as low as 6 mm. CFD simulations showed that straight grooves drastically reduce tangential particle velocity components, forcing powders to point towards the nozzle's focal point. A second batch of designs with a smaller nozzle angle (from 17° to 12°) focused on examining other groove geometries, including wider straight grooves and helical grooves. These simulations confirmed that narrow, straight grooves with uniform thickness provide improved powder focusing by controlling powder exit trajectories. In addition, helical grooves with steeper helical angles reduced the powder spray divergence. Finally, one control and the two best performing designs from each batch were manufactured and tested in a lab setting to experimentally observe the overall spray profile. Both the simulations and experiments showed an improvement in nozzle focusing with the addition of straight nozzle grooves, with experimental results showing a 17–18 % decrease in the spray width compared to the control nozzle.

1. Introduction

Direct Laser Metal Deposition (DLMD) is a spray-based additive manufacturing (AM) process that delivers powders to a substrate such that they can be fused together via a high-powered laser. To do this, a powder-gas mixture is supplied to a nozzle and ejected from one or more orifices such that the stream of powders intersects with the focal region of the laser beam used. The energy of the laser beam melts both the powders and the substrate below, creating a melt pool that cools and solidifies into a deposited layer as the deposition head (nozzle + laser) traverses along a predetermined path. Due to the relatively small size of the nozzle, the process can be manipulated using a Computer Numerical Control (CNC) machine [1] or a robotic arm [2], allowing for the manufacture of complex parts. This compact form also allows for this process to be integrated into machines that also incorporate subtractive manufacturing processes [3–5].

Because the nozzle directly supplies the powders to be deposited, the design of the nozzle plays an important role in determining the shape and resolution of the powder stream. As such, a variety of nozzle types have been designed, studied, and commercialized for the DLMD technique. Three categories of nozzles are often used to describe the common types of nozzle designs: Off-Axial [6], Discrete Coaxial [7], and

* Corresponding author.
E-mail addresses: tgabor@purdue.edu (T. Gabor), yun37@purdue.edu (H. Yun), sakin@purdue.edu (S. Akin), khkim@kimm.re.kr (K.-H. Kim), jkpark@kimm.re.kr (J.-K. Park), mbgjun@purdue.edu (M.B.-G. Jun).

https://doi.org/10.1016/j.jmapro.2022.08.039
Received 23 April 2022; Received in revised form 15 July 2022; Accepted 17 August 2022
Available online 6 September 2022

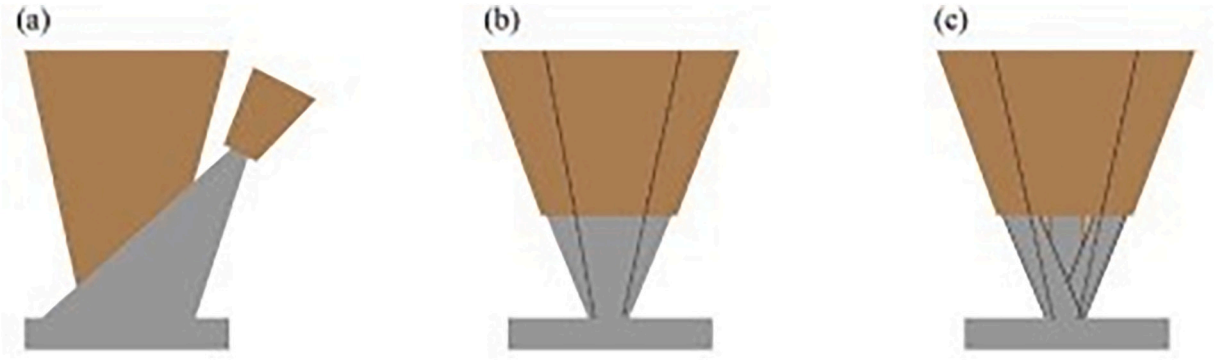

Fig. 1. DLMD Nozzle types: (a) Off-Axial, (b) Continuous Coaxial, (c) Discrete Coaxial [6].

Continuous Coaxial [6]. Each nozzle type is illustrated in Fig. 1. Off-Axial nozzles are characterized by a central laser beam positioned vertically above the substrate, often with a shield-gas nozzle positioned below the laser head to protect the equipment from rebounding powders. Powders are fed through a single nozzle not along the axis of the laser beam; this nozzle is angled such that the powder stream intersects with the laser such that a melt pool can be formed. The main drawback of this system is that deposition quality and efficiency is dependent on the deposition head's travel direction, often limiting the deposition process to a single direction [6,8].In addition, compared to Coaxial nozzles, the deposition efficiency suffers at higher powder feed rates [9].

Discrete and Continuous Coaxial (DC and CC) nozzles address the problem of off-axial nozzles by providing multiple sources of powder streams around the central laser beam axis. Discrete Coaxial systems involve the incorporation of multiple nozzles or orifices around the laser beam, each with an individual inlet and outlet such that the powder streams do not intersect within the nozzle [6]. Meanwhile, Continuous Coaxial nozzles distribute powder around an annular nozzle, with powder streams of multiple inlets coalescing into a single powder stream at the nozzle exit [6]. Oftentimes, a third annular exit is used to provide additional shield gas to the powder stream to ensure no oxidation occurs during the AM process. Both coaxial variants not only allow for omni-directional deposition, but also can allow for a more compact design as the powder feed is integrated around the laser head.

Out of all three nozzle types, Continuous Coaxial nozzles provide the highest potential for improving the DLMD process. A comparison between Off-Axial and Continuous Coaxial nozzles showed that the latter provided better overall deposition efficiency [9], whereas a comparison between Discrete Coaxial and Continuous Coaxial nozzle suggest improved deposition efficiency as well. The higher powder velocities provided by Continuous Coaxial nozzle ensured that more powders penetrated the melt pool rather than rebounding off the melt pool [10]. In addition, Continuous Coaxial nozzles can incorporate design features such as grooves [11,12], off-axis inlets [12–14], flow straighteners [13,14], and retraction/protrusion of nozzle inlets [15], along with other changes in both internal nozzle features and standard nozzle features such as nozzle angle and powder inlet angle. The flow of continuous coaxial nozzles, however, is more complex compared the other two types of nozzles, especially when there are numerous design features to add to the flow complexity. As such, it is important to understand the gas-powder flow within these nozzles and how changes to the nozzles' design affect both gas powder flow and deposition quality.

Initial Computational Fluid Dynamics (CFD) simulations of the DLMD process were done using a 2D-Axisymmetrical scheme [15,16], with the center axis located along the nozzle's center axis. The general profile observed shows a powder stream that converges to a single point, where there is a location with a minimum thickness and a maximum powder concentration. This stream then diverges again. The general profile is similar to analytical models used in the 90's [17,18]. Wen et al. [16] divides the sections of the powder stream profile into three parts: pre-"waist", "waist", and post-"waist". It is also observed that there can be multiple regions of high powder concentration, allowing for a range of stand-off distances to consider for operation. The location of this focusing or "waist" region is dependent on nozzle geometry [15] as well as the powder's coefficient of restitution [19,20] and powder size [20]. The introduction of the substrate also affects the location of maximum powder concentration, as rebounding powders will intersect with the powder stream a second time [21].

Although 2D-Axisymmetrical simulations gives a general understanding of the powder flow, a more in-depth understanding of the powder flow inside the nozzle is found when a full 3D model is simulated. Ibarra-Medina and Pinkerton [21] noted that when powders enter the nozzle via an inlet whose axis intersects with the central axis, it will impact the inner nozzle wall, resulting in the spreading of powders within the nozzle. This allows for a more even powder distribution within the nozzle, although it can be seen that concentration fluctuations correspond to powder inlet locations. Meanwhile, if the inlets are offset (do not intersect with the central axis), the powders will swirl around the nozzle, resulting in a diverging stream [13]. In addition, it has been noted that the powders will ricochet between the nozzle walls until they reach the nozzle exit, resulting in a variation of particle exit trajectories which affects the location of the peak powder concentration region [20].

Due to the ability to change the nozzle model easily in simulation, it is possible to investigate the impact of nozzle design on the powder spray process. One of the first simulation papers by Lin [15] investigated the effects of the relative configuration between the center nozzle exit and the annular powder exit on powder flow, with one configuration having the center exit protruding 2 mm from the nozzle tip, and the other having the center exit retracted 1 mm from the nozzle tip. It was determined that the retracted configuration created a focusing region closer to the nozzle tip (5 mm), whereas the protruded configuration created a focusing region father away (8 − 14 mm) from the nozzle tip.

J Zhang et al. [22,23] simulated and tested a continuous coaxial nozzle in lab scale, with inlet angles nearly matching the nozzle's angle. In addition, the outer wall of the cone was angled at 45°, and the inner wall at 39.9°. This design allowed for good powder distribution within the nozzle with only a few hot-spots. When analyzing the powder flow within the nozzle, the powder velocity range was shown to increase halfway into the nozzle. However, the exit powder velocity was shown to be affected by powder mass flow rate when it increased the average powder exit velocity. In addition, the exit powder flow was shown to have two concentration peaks, with the second determined to be a result of particle collision. Xia et al. [14] simulated a DLMD nozzle that incorporated an initial mixing chamber followed by a flow straightening section at different gas flow rates and powder feed rates. The flow straightening system allowed for even powder distribution within the nozzle. The nozzle showed risks of clogging right after the flow straightening section when low gas flow rates and high powder feed rates were supplied.

Another design aspect that was explored was the effect of nozzle

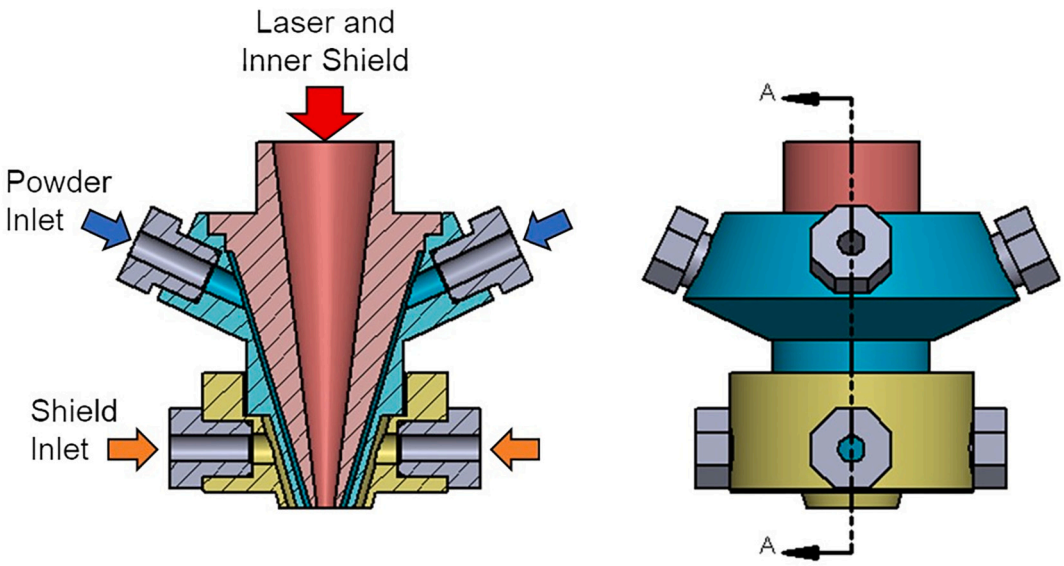

Fig. 2. Illustration of a typical continuous coaxial DLMD nozzle.

grooves that run along the inside of the nozzle. Arrizubieta et al. [11] proposed this solution in order to correct the powder trajectories from a swirling powder flow described earlier. This allowed for the powder flow to be focused again such that the powder stream intersects at the central axis. The authors of this paper also investigated the effects of grooves (both straight and tapered) on the nozzle's ability to focus the powder stream [12]. In addition, the effects of inlet angle and inlet offset were also examined. It was determined that 1 mm wide straight grooves provided the best focusing out of all nozzle configurations tested, irrespective of inlet angle and inlet offset. Straight grooves drastically reduced the tangential velocity component of the powders, ensuring that their exit trajectories were directed towards the nozzle's central axis; tapered grooves also provided better focusing, but less than the straight grooves. The configuration of the nozzle inlets mainly determined the overall powder distribution within the upper section of the nozzle before they are funneled into the grooves. Results from previously cited simulation models can be used as inputs for novel methods such as the one developed by Sobahanieh et al. [24] to help determine the effects of nozzle designs on laser attenuation and optimal nozzle standoff distance. In their paper, it was shown that an increase in powder feed rate would linearly increase laser attenuation, and that the optimal standoff distance should be where the powder stream and the laser focal length intersect in order to ensure the maximum energy transfer to the melt pool.

In this paper, DLMD nozzle design parameters such as nozzle angle, powder inlet angle, nozzle inlet offset, and internal nozzle groove geometry are studied using a combination of CFD and Design of Experiments (DOE) full factorial analysis. By focusing on studying the nozzle designs, it is possible to determine which design features will improve powder deposition efficiency and reduce powder waste through the improvement of powder focusing done by the nozzle. This will be done in two batches. In this study, the first batch of 12 designs are analyzed, characterized by input variable such as nozzle inlet angle, nozzle offset distance, and internal nozzle groove geometry. In addition, nozzle inlet pressure is used as a fourth input variable to provide a total of 24 cases all run in CFD simulation. Output parameters of powder cloud diameter, powder concentration, and max powder velocity are all obtained and analyzed from 10 mm below the nozzle inlet. Although DOE has been used to study and optimize the DLMD process, the focus of these studies have been on process parameters such as with Moradi et al. [25] – studying scanning speed, scanning pattern, and powder feed rate – and with Nankali et al. [26] – studying laser power, laser focal plane location, and scanning speed. In addition, the outputs focus on deposition quality metrics such as deposition height, deposition width, surface smoothness, geometric stability, and micro hardness. In the second batch, four more designs are analyzed in CFD, this time focusing on understanding how nozzle groove geometries not covered in the first batch control powder exit trajectories. Finally, the best design from beach batch (i.e. the ones that focus the powder the most) were manufactured alongside a control design, and their powder flows were examined experimentally to validate the CFD models.

Table 1
All design permutations that were tested. Each design was simulated at 2 different inlet conditions: 1 kpa and 10 kpa for both shield and powder inlets.

Design	Powder inlet angle (°)	Inlet offset (mm)	Grooves (#)	Groove type
1	0	0	0	None
2	0	10	0	None
3	25	0	0	None
4	25	10	0	None
5	0	0	12	Straight
6	0	10	12	Straight
7	25	0	12	Straight
8	25	10	12	Straight
9	0	0	12	Tapered
10	0	10	12	Tapered
11	25	0	12	Tapered
12	25	10	12	Tapered

2. Nozzle designs

The overall base construction of the nozzle consists of three different parts, which can be seen in Fig. 2. The outer section, colored yellow, is mainly used to provide shielding gas to protect the powder stream, and screws onto the middle section (blue). This middle section is used to provide a mixture of powder and nonreactive gas such as Argon or Nitrogen, and screws into the inner section colored red. The innermost section is used to provide a pathway for the laser beam as well as protective inner gas to protect the laser from powder reflection into the nozzle. As for a continuous coaxial (CC) nozzle, a gap is provided in between each section for where the gas and powder flow through the nozzle and exit out the bottom, with each stream separated by a thin wall.

The creation and simulation of nozzle designs were done in two

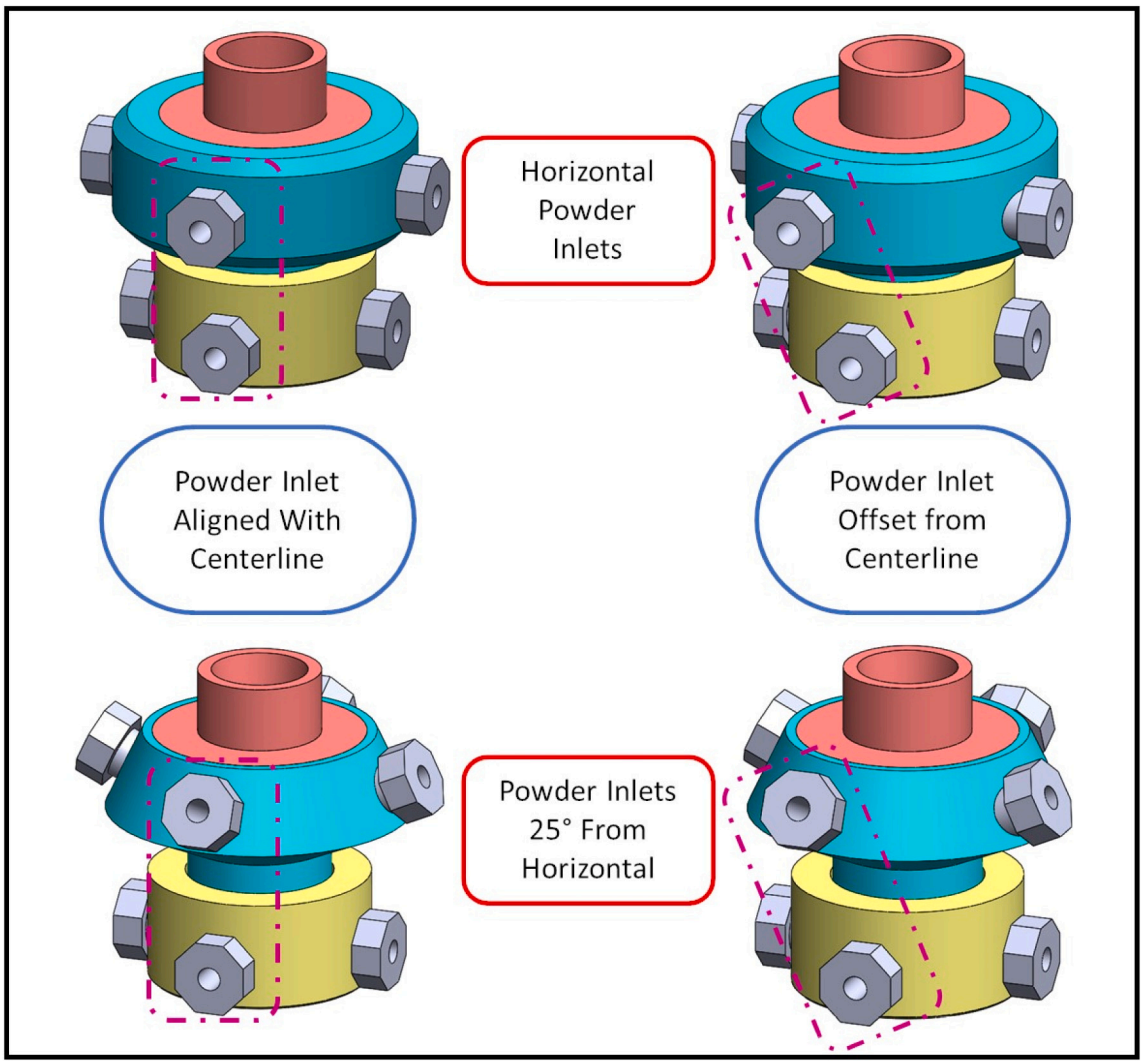

Fig. 3. Variations in powder inlet position used for simulating the first batch of designs.

batches. The first one focused on 3 different design parameters and two inlet pressures (1 kPa and 10 kPa), which is outlined in Table 1. The configurations for the nozzle inlets, shown in Fig. 3, are only used in the first batch of simulations. Because the inlets are the locations where powders enter the nozzle chamber, it is important to examine how changes in the nozzle inlet affects powder distribution, velocity, and focusing. An inlet trajectory that is more closely aligned to the nozzle exit angle will allow the powders to more easily flow into the nozzle, but may affect annular powder distribution as the majority of powders will stick closer to the nozzle outlet. Meanwhile, offsetting nozzle inlets from the center-line will force the gas and powders to swirl around the nozzle until they exit, which may provide either beneficial or detrimental effects to the nozzle's ability to focus depending on the powders' weight and the strength of the gas flow.

The last design parameter is created by making groove patterns on the outer cone face of the part colored in red in Fig. 2. The protruding sections of the modified cone sit flush with the inner face of the middle part, which in turn restricts the gas-powder mixture to flow into the grooves towards the exit. By changing the groove design, it is possible to affect the powders' exit trajectory and in turn the nozzle's ability to focus. As such, a total of nine variations of this part (one without grooves and eight with grooves) were created, all shown in Fig. 4. In Batch 1, two of the variations were designed specifically to better accommodate for the induced swirling flow from the offset inlets, while the rest were designed with centered inlets in mind. All grooved nozzles contain a total of 12 grooves evenly spaced apart, with each ending in a 1 mm × 1 mm profile at the nozzle tip.

Due to the large number of varying conditions in Batch 1, a full factorial analysis was used, with the parameters outlined in Table 2. A total of 4 factors and 9 levels were used, with the groove type having 3 levels instead of 2 as there were three different groove configurations to be tested and analyzed. From there, an analysis of variance (ANOVA) was performed, with the results outlined more in Section 5.

In Batch 2, the nozzle exit angle was changed to 12° compared to the previous 17°exit angle, as this new profile would allow for an overall more compact design than the previous batch. Aside from this, the only design aspect that changed was the groove shape. Two designs (13 and 14) were focused on comparing groove width (1 mm wide vs 1.5 mm wide). It is important to note that the number of grooves in design 14 is 8 compared to the more common 12. This change was made out of necessity, as each set of grooves still needed a reasonable amount of wall spacing between each other to be reasonably manufacturable while still keeping the nozzle exit width the same. The other two nozzles (15 and 16) examined helical groove patterns. These helical patterns are a more controlled way to induce a swirling flow in the nozzles, as the shape of the grooves affects the tangential velocity component of the powders while reducing the overall variation in powder trajectories.

Once both batches were simulated, a total of three DLMD nozzle designs were selected to be prototyped and tested, which are shown in Fig. 5. Nozzle A in Fig. 5 was set as the control, while Nozzles B and C

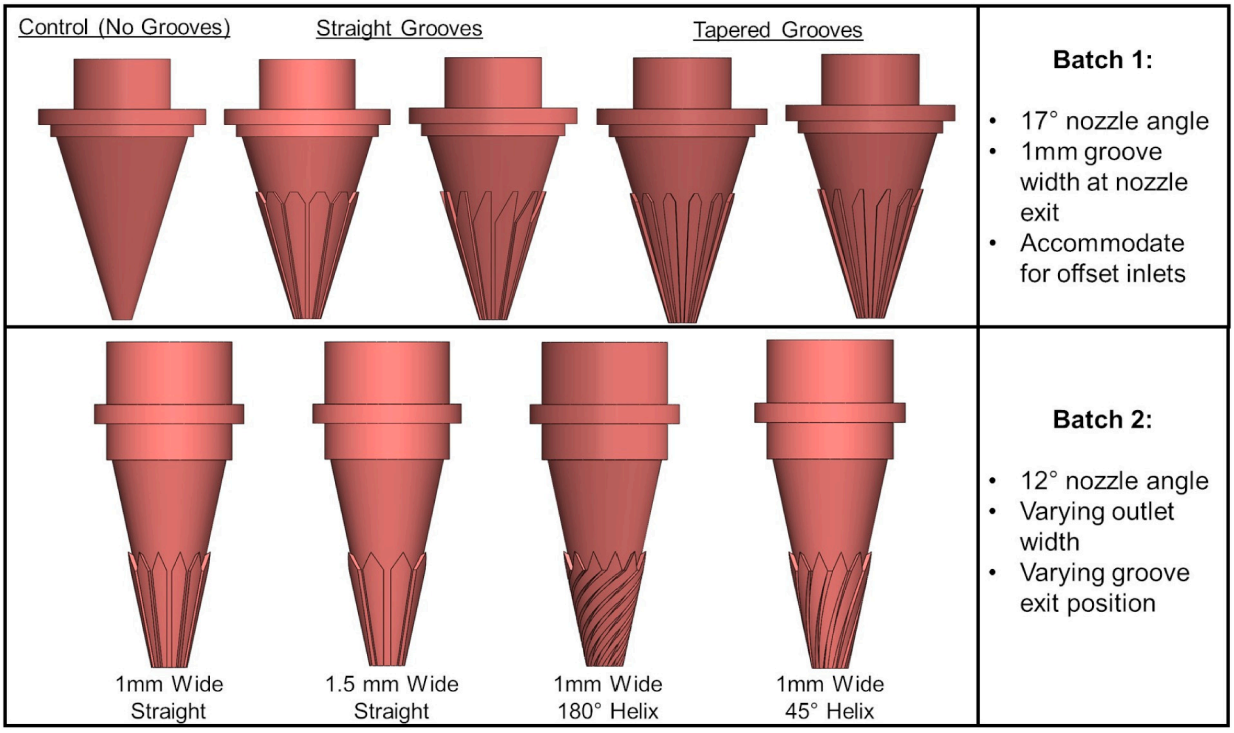

Fig. 4. Variations of the innermost nozzle part that defines the powder flow trajectory in the nozzle for both Batch 1 and Batch 2.

Table 2
Full factorial design for the analysis of the nozzle designs.

Factors	Factor codes	# of levels	Levels	Level values
Inlet pressure (Pa)	A	2	−1,1	1000, 10,000
Inlet angle (°)	B	2	−1,1	0, 25
Inlet offset (mm)	C	2	−1,1	0, 10
Groove type	D	3	−1,0,1	Straight, none, tapered

were selected from Batches 1 and 2, respectively. Nozzle A is similar to many commercial continuous coaxial nozzles, with a completely annular profile throughout the nozzle chamber. Therefore, this nozzle is viewed as the control in this study, with Nozzles B and C compared and contrasted in reference to Nozzle A. Nozzle B differs from Nozzle A mostly via the addition of grooves on the inner cone of the nozzle. The raised sections lay flush with the outer wall of the nozzle, producing twelve channels that the powders are forced to pass through to the exit. The grooves run all the way to the nozzle exit, producing twelve 1 mm × 1 mm wide exits placed radially along the nozzle exit. To facilitate the funneling of powders into the grooves, the geometry includes a set of v-shaped channels that lead into each groove. Aside from the grooves, Nozzle B is unique in that this nozzle is made of brass instead of steel to assist in heat dissipation during the DLMD process.

Nozzle C differs from both Nozzle A and Nozzle B in a variety of ways. Firstly, the nozzle angle is steeper, measuring at 12° from the vertical compared to 17° from the vertical for the other two nozzles. This was done to provide a more compact form. In addition, the nozzle inlets are angled at 50° compared to 25° from the horizontal. The groove geometry also varies in a few minor ways compared to Nozzle B. Firstly, the grooves are shorter, measuring 25 mm compared to Nozzle B's 30 mm. The top of the raised section is also rounded, providing a different profile for the powders to funnel into the nozzle structure. Finally, due to manufacturing constraints, the grooves start out with a 1 mm width and

Fig. 5. Prototyped versions of each nozzle that were both simulated and tested experimentally.

Table 3
Outline of differences in design features of each nozzle.

Nozzle	A	B	C
Nozzle angle	17°	17°	12°
Features	No grooves	Straight grooves	Slightly tapered grooves
Top groove width	N/A	1 mm	1 mm
Bottom groove width	N/A	1 mm	0.5 mm

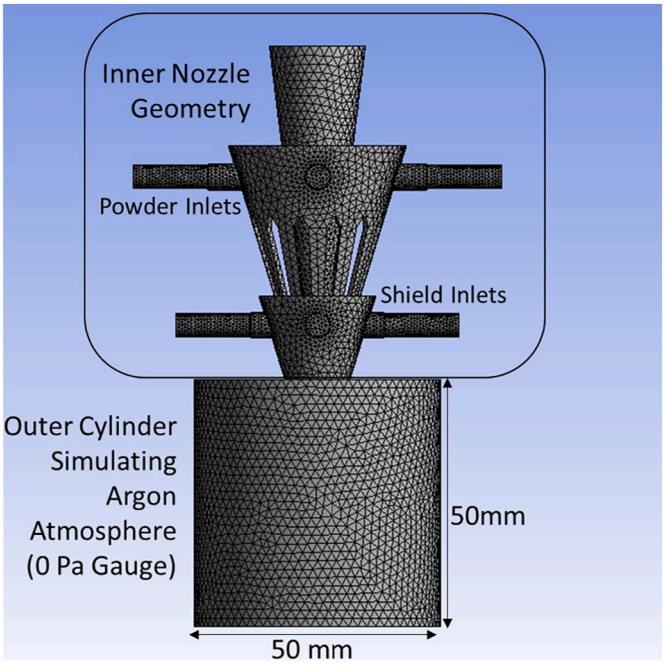

Fig. 6. Example of the meshed simulation domain for Nozzle B.

Table 4
Material properties used in the simulations of the nozzles.

Gas material	Gas density (kg/m^3)	Gas viscosity (kg/ms)	Powder material	Powder density (kg/m^3)
Argon	1.6228	2.13e-05	Copper	8978

end with a 0.5 mm width, resulting in a small taper. A summary of the differences between each nozzle is outlined in Table 3.

3. Simulation setup and theory

In the simulation, ANSYS Fluent 19.2 was used to perform 3D CFD simulations of each nozzle. The inside geometry was created in reference to each nozzle's CAD model, with each nozzle inlet set at 1–10 kPa of gas pressure. To simulate a free-stream environment, a 50 mm × 50 mm cylinder is attached to the nozzle's exit tip, with the boundaries set to atmospheric pressure. An example of the meshed domain is shown in Fig. 6. The entire domain is assumed to be consisting of only argon atmosphere, whereas the powders simulated are all copper. The specific values of each material are outlined in Table 4.

To perform the simulations, the conservation of mass, conservation of momentum, and standard k-ε turbulence equations were used. These equations are calculated using the 3D time invariant versions [27]. The conservation of mass equation is used is:

$$\frac{\partial u}{\partial x}+\frac{\partial v}{\partial y}+\frac{\partial w}{\partial z}=0 \tag{1}$$

where u, v, and w are the gas velocities in the x, y, and z cardinal directions, respectively. Essentially, the change in gas density over time must be a result of gas entering or exiting the domain that is examined such that no mass is lost.

The conservation of momentum equations used are:

$$\rho\left(u\frac{\partial u}{\partial x}+v\frac{\partial u}{\partial y}+w\frac{\partial u}{\partial z}\right)=-\frac{\partial P}{\partial x}+\mu\left(\frac{\partial^2 u}{\partial x^2}+\frac{\partial^2 u}{\partial y^2}+\frac{\partial^2 u}{\partial z^2}\right)+\rho g_x+F_x \tag{2}$$

$$\rho\left(u\frac{\partial v}{\partial x}+v\frac{\partial v}{\partial y}+w\frac{\partial v}{\partial z}\right)=-\frac{\partial P}{\partial y}+\mu\left(\frac{\partial^2 v}{\partial x^2}+\frac{\partial^2 v}{\partial y^2}+\frac{\partial^2 v}{\partial z^2}\right)+\rho g_y+F_y \tag{3}$$

$$\rho\left(u\frac{\partial w}{\partial x}+v\frac{\partial w}{\partial y}+w\frac{\partial w}{\partial z}\right)=-\frac{\partial P}{\partial z}+\mu\left(\frac{\partial^2 w}{\partial x^2}+\frac{\partial^2 w}{\partial y^2}+\frac{\partial^2 w}{\partial z^2}\right)+\rho g_z+F_z \tag{4}$$

In the above equations, F represents force terms such as gravity, influence from particles, etc. ρ is again the gas density, μ is the gas viscosity, u, v, and w are gas velocity components in the x, y, and z components, respectively, and P is the gas pressure.

One of the more common sets of equations used for turbulence are the standard $k-\varepsilon$ equations, developed by Launder and Spalding [28]. It is important for flows with high Reynolds numbers ($Re > 4000$ for a pipe, where $Re = \rho vL/\mu$ with L being a characteristic length or diameter). The turbulent kinetic energy (TKE) equation:

$$\frac{\partial(\rho k v_i)}{\partial x_i}=\frac{\partial}{\partial x_j}\left[\frac{\mu_t}{\sigma_k}\frac{\partial k}{\partial x_j}\right]+2\mu S_{ij}S_{ij}-\rho\varepsilon \tag{5}$$

The TKE Dissipation rate equation:

$$\frac{\partial(\rho\varepsilon v_i)}{\partial x_i}=\frac{\partial}{\partial x_j}\left[\frac{\mu_t}{\sigma_\varepsilon}\frac{\partial \varepsilon}{\partial x_j}\right]+2C_1\frac{\varepsilon}{k}\mu S_{ij}S_{ij}-\rho\varepsilon-C_2\rho\frac{\varepsilon^2}{k} \tag{6}$$

where k is the turbulent kinetic energy, ε is the TKE rate of dissipation,$S_{ij}=\frac{1}{2}\left(u_{ij}+u_{ij}\right)$ is the fluid strain rate tensor, the total viscosity is defined.

by $\mu=\mu_t+\mu_l$ where μ_l is a fluid's laminar viscosity, and $\mu_t=\rho C_\mu k^2/\varepsilon$ is the turbulent viscosity. In addition, there are five constants that were determined empirically [27,28] that are used in the standard $k-\varepsilon$ model:

$C_1=1.44$, $C_2=1.92$, $C_\mu=0.09$, $\sigma_k=1.0$, and $\sigma_\varepsilon=1.3$. σ_k and σ_ε are the Prandtl numbers for k and ε, respectively.

To simulate the powder flow, a Lagrangian approach is used. It was determined by Wen et al. [16] that the low concentration of powder within the flow allows for the use of this method. The force balance equation used for the powder flow is as follows:

$$m_p\frac{d\vec{v_p}}{dt}=C_D\rho\left(\vec{v}-\vec{v_p}\right)\left|\vec{v}-\vec{v_p}\right|\frac{A_p}{2}+\frac{\vec{g}\left(\rho_p-\rho\right)}{\rho_p}+\vec{F} \tag{7}$$

where m_p is the mass of the particle, v_p is the particle velocity, C_D is the particle's drag coefficient, A_p is the particle's cross-sectional area, g is gravity, ρ is the particle's density, and F represents all other forces acting on the particles. One of the important forces that will be considered in many simulations in this paper is the momentum transfer between particles and the shield gas, as both powders and gas influence each other in the flow. This transfer force F_p is as follows:

$$F_p=\sum\left(\left(\frac{18\mu C_D Re}{\rho_p d_p^2 24}\left(v_p-v\right)+F_{other}\right)\Big/\,Dotm_p\Delta t\right) \tag{8}$$

where d_p is the particle diameter, F_{other} represents any other force transferring momentum to the particles, m_p is the powder mass flow rate, and t is the time step.

Various drag coefficient models have been presented over the years in order to provide a model that allows for a better understanding of powder flow through various apparatuses. One of the most common methods used was an equation developed by Morsi and Alexander [29], which assumed the particles are spherical. This equation is used for all simulations within this paper. The equation is as follows:

$$C_D=a_1+\frac{a_2}{Re}+\frac{a_3}{Re^2} \tag{9}$$

where a_1, a_2, and a_3 are all curve-fitting constants that are outlined in [29], each one varying based on the flow's Reynolds number.

Finally, to simulate the powders, a Rosin-Rammler particle distribution is implemented:

Table 5
Parameters for the simulated Rosin-Rammler Distribution.

Min diameter (μm)	Max diameter (μm)	Average diameter (μm)	Spread parameter	Number of diameters
15	50	32.5	3.5	10

$$F_d = exp\left[-\left(\frac{d}{\bar{d}}\right)^n\right] \tag{10}$$

where F_d describes the powder mass fraction of particles greater than a given particle diameter d, $\bar{d}$ is the average particle diameter, and n is the particle spread parameter. The specific particle distribution parameters used are listed in Table 5.

4. Experimental setup

The nozzles were tested in a free stream condition so that they can be compared to the simulation results, as shown in Fig. 3. Each nozzle was set up in a 3D-printed stand, with the tip of the nozzle clearly visible underneath the stand. Copper powders were stored and supplied via a Colombia Coatings powder keg and pump [30], with 100 psi of air supplied to the air intake to be regulated by a set of 3 valves until a consistent powder flow was produced. A metal tray was used to capture and conserve powders for repeated testing. The overall focus was observing the shape of the powder spray produced and comparing that with the simulated results, as the nature of this test is less precise than others available. A Canon EOS Rebel T7 was used with a 75-300 mm f 1:4–5.6 zoom lens, and was focused on the powder spray, which was lit by a side light that the powder stream was visible.

To measure the shape of the spray, each image was examined with image processing software (ImageJ). All three nozzles have a tip diameter of 10 mm, and therefore can be used as a reference in order to determine the size of spray parameters such as spray width, height of the spray "waist," and distance at which the powders begin to converge. To mitigate variance, a total of 8 to 11 images were captured for each nozzle. Spray width at the observed thinnest point was measured with each image, then averaged to estimate the average focused spray width.

5. Results and discussion

5.1. Analysis of design features

In order to understand the impact of the design features outlined in Table 2, three parameters were chosen for analysis: (i) the highest powder concentration value obtained from the simulation, (ii) the diameter of the measured particle cloud in simulation, and (iii) maximum particle velocity magnitude. All of these values were obtained from a distance from 10 mm away from the nozzle tip, as this was representative of a typical standoff distance for the DLMD process and allowed for a common measuring point between all 24 cases. The maximum powder concentration shows what the expected powder concentration will be at the center of a focused powder spray, providing a good idea of how much of the laser beam will be absorbed by powders. As shown in Fig. 7a, the powder concentration decreases as inlet pressure increases. This is understandable in a steady-state simulation, as higher pressure corresponds to higher powder velocity, which in turn means that the powders have less time to linger within a given volume cell. The only exceptions to this are specifically nozzles 2 and 4, which have no grooves but have offset inlets.

Particle cloud diameter, shown in Fig. 7b, is obtained by measuring the diameter of the region that is 10 % of the maximum concentration value. Although this diameter is generally larger than the majority of laser diameters used in the DLMD process, it allows for an overall better picture of the spray profile. Maximum concentration and cloud diameter in tandem provide a clear visual of which nozzle design features improve DLMD powder spray focusing. As seen with nozzles 5–8, 11, and 13, nozzles with high powder concentration (above 25 kg/m^3) have very low particle cloud diameters, indicating good spray focusing. Nozzle 7 is the best of the entire batch in this case, with the highest powder concentration and the lowest (and most consistent) particle cloud diameter. Meanwhile, nozzles 2 and 4 have the largest spray diameters and the lowest particle concentration, irregardless of pressure, indicating that nozzles with offset inlets that have no way to change particle trajectory internally before they exit will not be able to focus powders.

Examining the simulated particle trajectories only further corroborated the results shown in Fig. 7. In general, the particle behavior can be split into 4 distinct categories, which are outlined in Fig. 8. The first category involves designs (1 and 3) that have no internal geometry as well as inlets that point towards the nozzle's central axis. Although all designs have powders impacting the central wall upon entering the chamber, these designs do not have any way to correct for particle spreading inside the nozzle, which can be seen in Fig. 8a. The resulting exit trajectories show that although most of the powder stream is focused, stray particles that gain a tangential velocity component due to internal spreading do not focus.

A high tangential velocity component is what defines the second category (designs 2 and 4), which have offset inlets that induce a swirling gas-powder flow. Fig. 8b clearly demonstrates that high tangential velocity component results in powders that exit the nozzle away from the nozzle's central axis and thus do not focus. This behavior

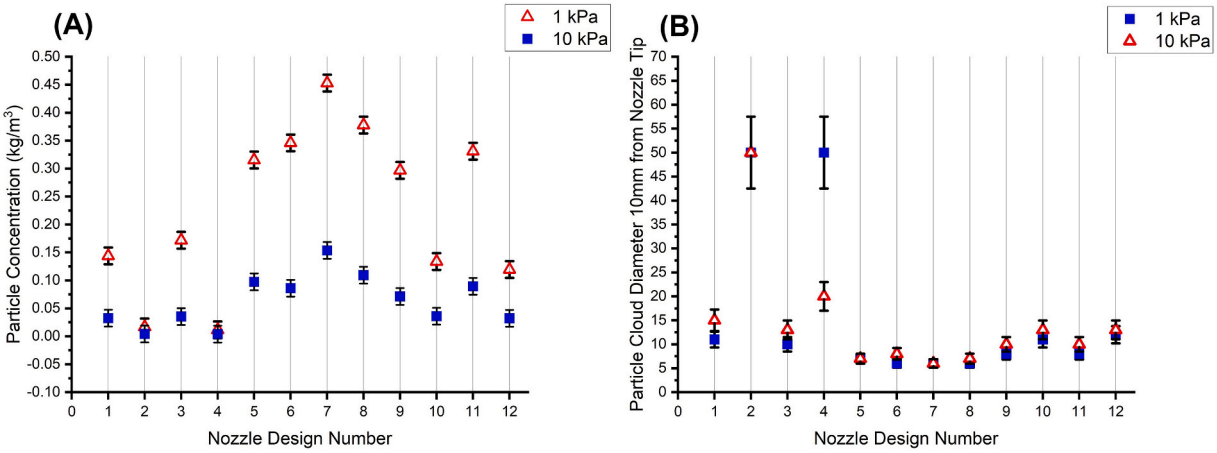

Fig. 7. (A) Maximum particle concentration and (B) Particle Cloud Diameter of the first batch of nozzles, measured from 10 mm from the nozzle tip.

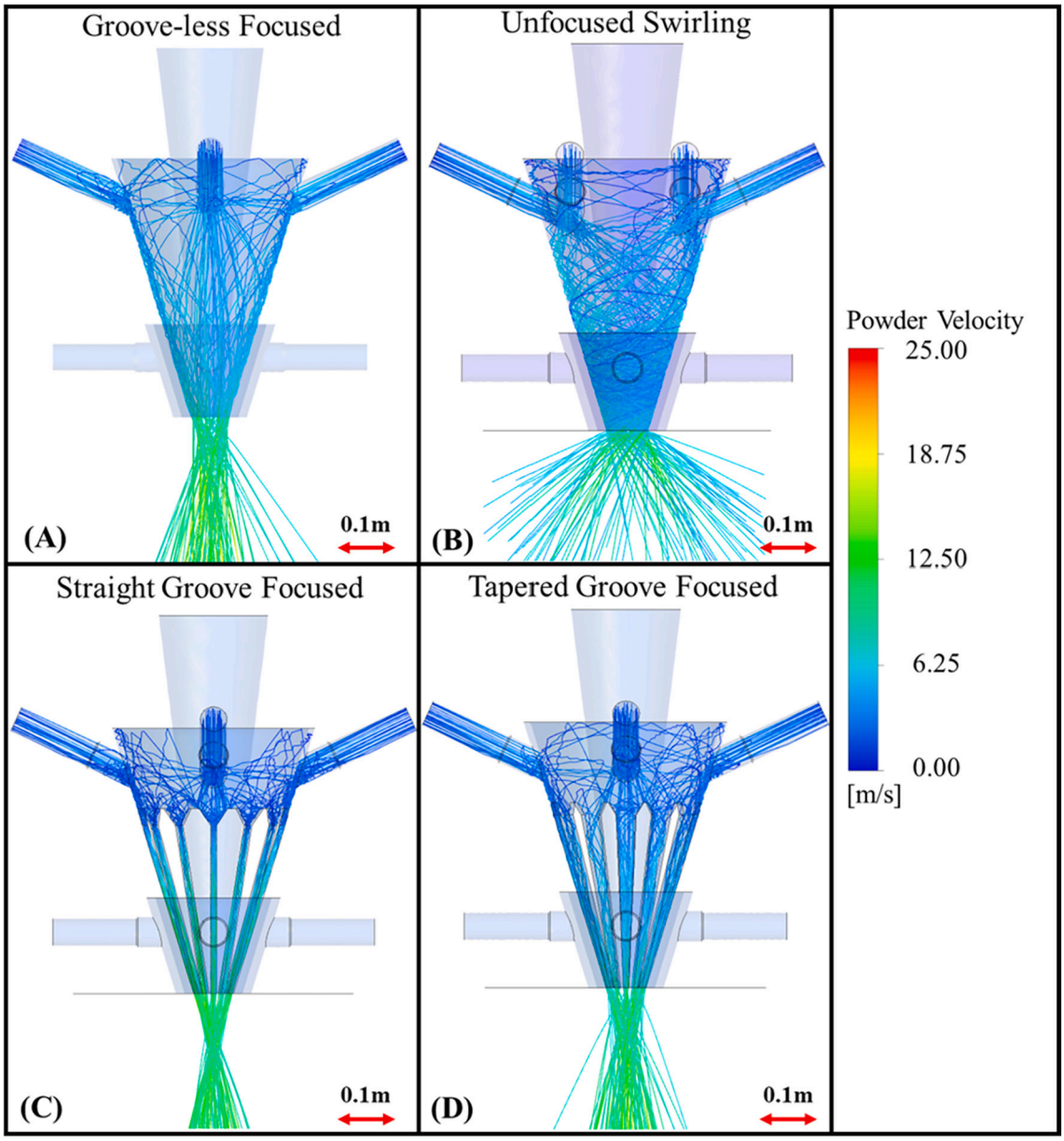

Fig. 8. The four general spray shapes that appeared in the first batch of simulation trials: (A) semi-focused spray from nozzles without grooves and without offset inlets, (B) unfocused spray from offset inlets, (C) highly focused spray from straight grooved nozzles, and (D) focused spray from tapered grooved nozzles.

explains the large particle cloud diameter measured in Fig. 7b, as this type of design does not focus the powders. This behavior indicates a high Stokes Number, which indicates that the particles tend to separate from the gas flow as the gas flow is not strong enough to force the heavy metallic powders to follow it. The Stokes Number is generally calculated by:

$$Stk = \frac{\rho_p d_p^2 u_0}{18 \mu_g l_0} \tag{11}$$

where ρ_p is the particle density, d_p is the particle diameter, u_0 is the gas velocity far away from a given obstacle or geometric change, μ_g is the gas viscosity, and l_0 is the flow's characteristic length. For the smallest particle diameter of $15\mu m$, a gas velocity of 10 m/s (the lowest maximum gas velocity shown in Fig. 9), and a characteristic length of $1mm$ (the shortest distance between the inner nozzle walls), the Stokes Number is calculated to be 52.7. This high stokes number means that particle motion is highly dictated by the particle's momentum and interaction within the nozzle walls. In all simulations, particles bounce between the nozzle walls as they travel towards the exit, and then follow their exit trajectory.

The final two design categories from batch 1 all have internal nozzle geometry that forces the powders to exit the nozzle towards the central axis. The third category consists of all nozzles with straight grooves (Fig. 8c), whereas the fourth consists of all nozzles with tapered grooves (Fig. 8d). Comparing these two categories, the nozzles with straight grooves consistently focus all the powders, whereas the nozzles with tapered grooves show improved focusing compared to nozzles without grooves, but are not as effective as the straight groove case. This effectiveness is best illustrated in Fig. 9a-b, where straight grooves consistently have the lowest concentration diameter and the highest peak concentration values, tapered grooves showing slightly higher concentration diameters and peak concentration values compared to the no groove cases, and no grooves showing the highest variation in diameter depending inlet position while also having the lowest peak concentration values for any offset value greater than zero.

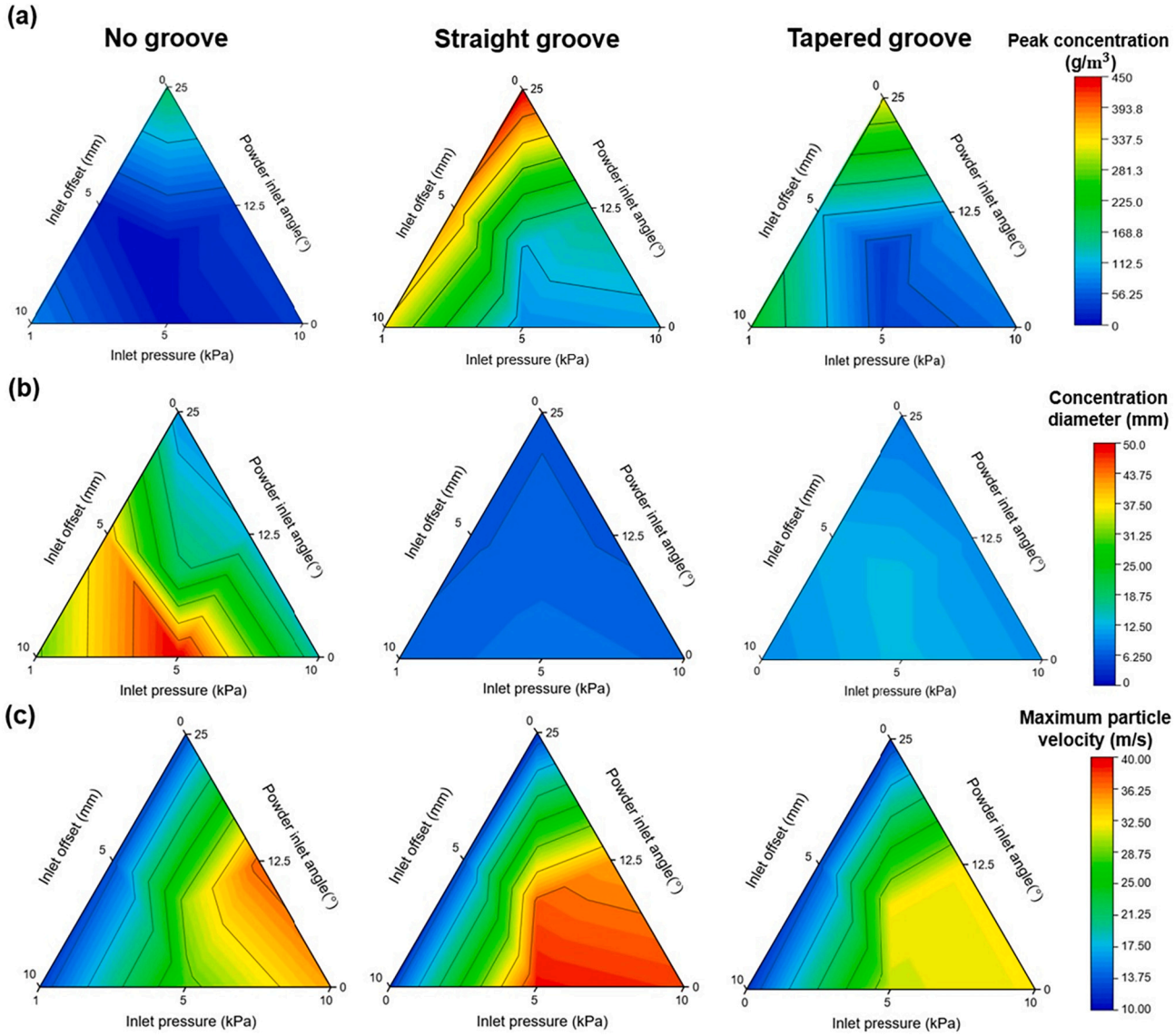

Fig. 9. The relationship between the factors in Table 2 for (A) Peak particle concentration, (B) Particle cloud diameter, and (C) Maximum particle velocity.

The effectiveness of straight grooves is largely due to their ability to reduce the tangential velocity component of the powders. Constant collision with the groove walls result in the particles being redirected towards the nozzle exit, while the force the gas exerts onto the powders increase the powder's velocity vector in that direction. The tapered grooves, while still subjecting powders to a narrow stream of gas, do not reduce the tangential velocity component of the powders quickly enough, as the powders have more time to travel within the grooves between bounces. This results in reduced focusing effectiveness compared to straight grooves.

The presence of grooves also has a strong effect on particle velocity, as demonstrated in Fig. 9c. The highest velocity values are all achieved with straight grooves with high inlet pressure, regardless of inlet offset. Similar behavior is found with nozzles with tapered grooves, but the maximum velocity is around 10 *m/s* less than the straight groove case. Groove-less nozzles show a less drastic correlation between velocity and pressure. In nozzles with grooves, the cross sectional area in the nozzle chamber is either gradually or abruptly reduced (depending on the groove shape), and this continues up to the nozzle exit which also has a reduced cross sectional area compared to the groove-less designs. A reduction in this area will always result in an increase in gas velocity as the volumetric flow rate through the nozzle must say the same. This increase in velocity corresponds to an increase to the force acting on the powders, thus accelerating the powders to higher velocity. The abrupt change in this cross sectional area in straight grooves corresponds to a stronger increase in velocity and therefore a stronger force on the powders.

Further analysis of the ternary plots in Fig. 9 shows another correlation between inlet angle, powder focusing, and velocity. In all cases, a steeper inlet angle corresponds with a higher peak powder concentration, a lower concentration diameter, and a lower maximum particle velocity, with the reverse corresponding to a more shallow inlet angle. Although the sample sizes are somewhat small for each case, these correlations do still make sense. In the case of peak concentration and concentration diameter, the steeper inlet angles are more aligned with the overall nozzle angle. This means that the powders in the nozzle do not spread as much within the nozzle upon impacting the nozzle wall, in turn reducing the average powder's tangential velocity component. The larger inlet angle also reduces the time the powders stay within the nozzle, as they already have a stronger velocity component that is in line with the nozzle angle. This means that the powders spend less time within the chamber of the nozzle, reducing the amount of time the powders accelerate.

Once the effectiveness of straight grooves were established, a new

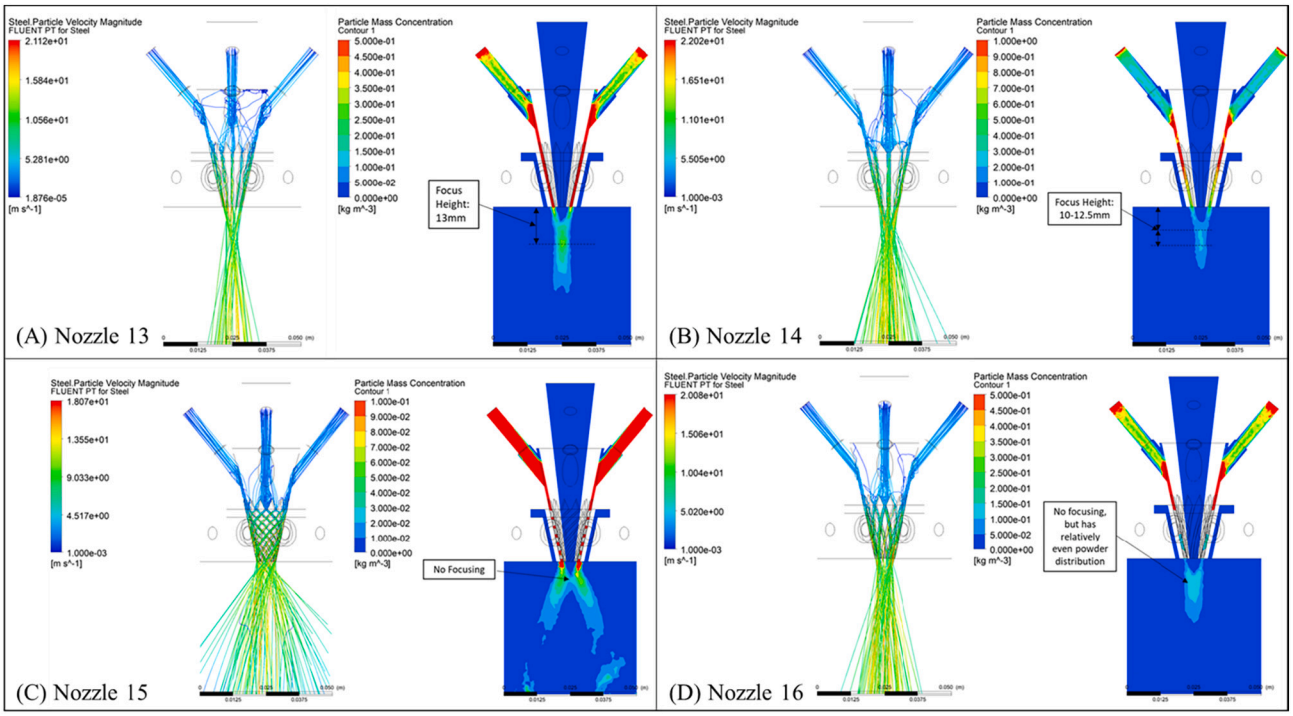

Fig. 10. Simulation results of the second batch of simulation trials: (A) 1 mm × 1 mm wide straight grooves, (B) 1.5 mm × 1 mm wide straight grooves, (C) helical grooves with a shallow helix angle, (D) helical grooves with a steep helix angle.

batch of nozzle designs were created to explore different variations in groove design as well as a change in nozzle angle. This simulation results of the second batch of nozzles is shown in Fig. 10. The first point of comparison is between nozzles 13 and 14, which vary the groove width. The wider grooves in nozzle 14 result in a spray that is slightly wider compared to nozzle 13, resulting in a lower peak concentration at the focusing region. Similar to the tapered grooves of designs 9–12, the powders have more room to travel in the lateral direction compared to the narrow grooves, meaning that the tangential velocity component is greater once the powders exit. Still, wider grooves may be a viable option to reduce powders clogging within the grooves without complicating the nozzle geometry even further, and thus may be a candidate for future investigation.

The final two nozzle designs, 15 and 16, were made to determine if controlling the tangential velocity component could produce desirable effects. The shallow helical angle of the grooves in nozzle 15 produced results to designs 2 and 4, but with a reduced outer spray width. This angle was still too great to provide any proper focal point for the laser to melt powders onto, and as such is not a desirable design. Nozzle 16, however, produced unique results. With a steep helical angle, the powders produced a spray that provided much more even powder distribution in a large area of the spray. Although grooves do not allow for much variation in powder trajectory, there is still some variation present due to the stochastic nature of powder sprays. With a steep helix angle, the powder sprays from each groove overlap slightly to produce an wide spray pattern of more even concentration. Although design 16 is not focused, this spray pattern could be useful for applications that desire a more even powder spray distribution. In addition, the reduction in powder concentration will reduce effects of laser attenuation. If powder feed rate is needed to be higher and waste is not as much of a concern, then design 16 may be beneficial in some applications of DLMD. In addition, if the laser beam is both wide and powerful, then this type of design may allow for wider deposited layers, reducing time that the DLMD system needs to operate at the cost of spray resolution. This paper

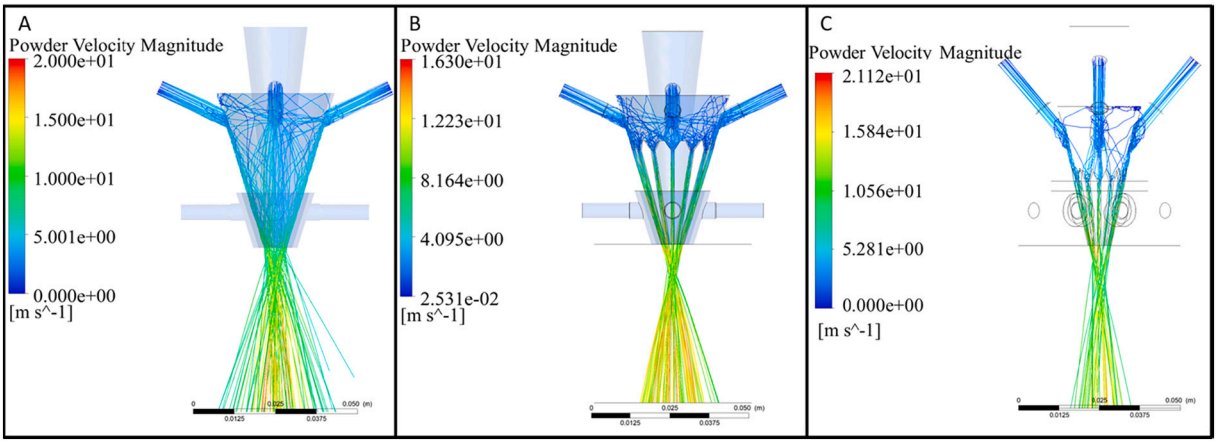

Fig. 11. Trajectory of particle streamlines for each nozzle, each colored with the particle velocity value based on the particles' position on the path.

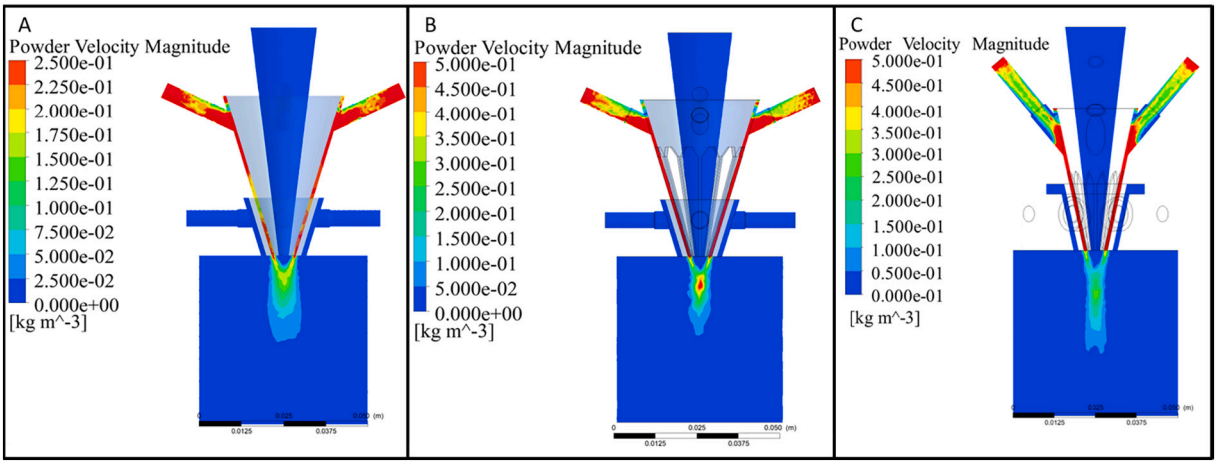

Fig. 12. Particle concentration contours for each Nozzle.

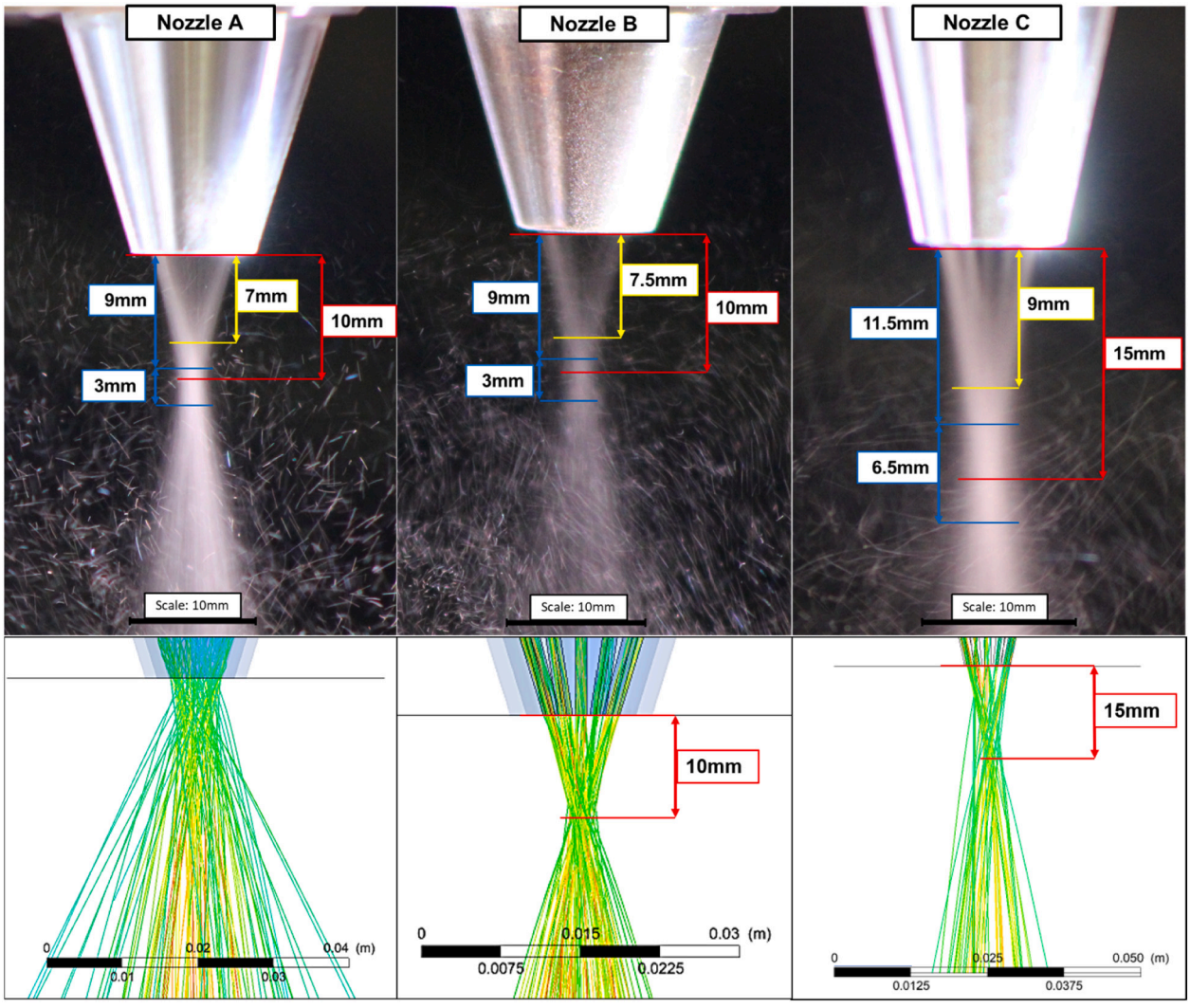

Fig. 13. Experimental spray profiles of each nozzle (top panel), compared with their simulated counterparts (bottom panel).

focuses on improving DLMD spray focusing, and as such design 16 was not considered in the experimental validation stage.

5.2. Simulation of manufactured nozzles and experimental validation

Examining the powder stream trajectories of each nozzle, as shown in Fig. 11, it is clear that Nozzle A does not focus as well as Nozzles B and

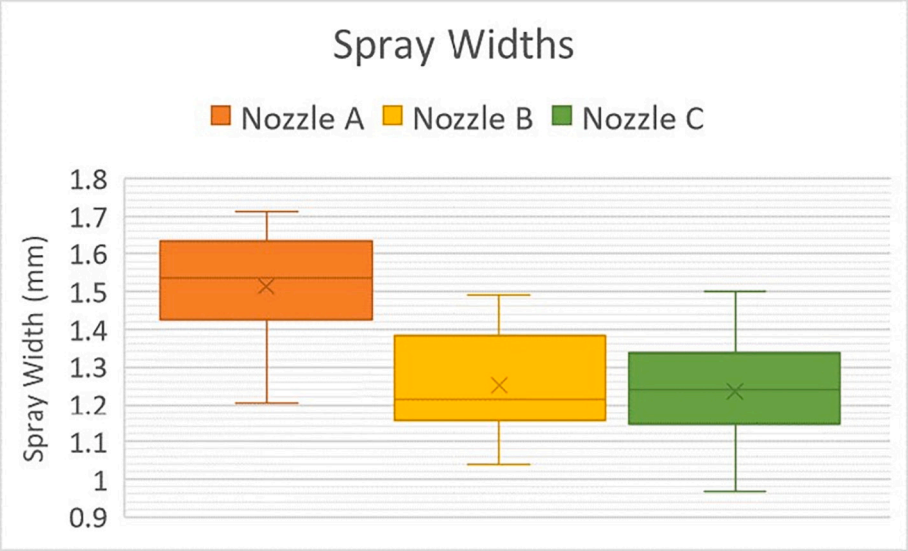

Fig. 14. Ranges of measured spray widths for each nozzle.

C, with multiple powder path lines diverging from the overall nozzle focus. It is important to note that Nozzle A and Nozzle B share all but one geometric design feature, the presence of flow-straightening grooves. This can easily be attributed to how the powders travel within the nozzle. While the majority of the powders exit the nozzle wall and flow downward, many powders also travel in unintended directions, gaining a tangential velocity component that is not fully reduced by the time the powder exit the nozzle. The initial powder flow characteristics of Nozzles B and C are also very similar to Nozzle A, where the powders impact the inner wall of the nozzle and spread outwards. The steeper inlet and nozzle angle of Nozzle C does show a small reduction of powder spreading, but does not eliminate it and the tangential velocity component. What does eliminate the tangential velocity component, however, is the addition of grooves in Nozzles B and C. The grooves force the powder trajectories to follow the geometric path to the nozzle exit, resulting in improved focusing with a large reduction of powder deviance.

Similar to the particle streamline results, the particle concentration maps in Fig. 12 show where and how well each nozzle focuses the powders. Nozzle A, with no grooves, does appear to have a focusing region starting at the 8 mm mark and ending at around the 11 mm mark, with the overall shape of the powder stream being wider than Nozzles B and C. This indicates that the powders are less focused without the addition of grooves. Nozzle B, on the other hand, has a highly defined focusing region at the 9-12 mm range, with powder concentrations reaching above 0.5 kg/m^3. This concentration value is even higher than the peak concentration of Nozzle C. This can be attributed to larger range of powder focusing shown in the contour, with a peak located at around 13 mm from the nozzle tip. The steeper nozzle angle reduces powder concentration peaks as the powder spray is more spread out throughout the spray profile.

Experimental results of Nozzle A, as seen in Fig. 13, shows the powder streams begin to converge at around 7 mm from the nozzle tip, with the thinnest point of the spray located at around 10 mm. The ideal focus region is located between 9 mm and 12 mm from the nozzle tip, around the location of the thinnest region. The spray profile of Nozzle B is similar to spray profile to Nozzle A, with the thinnest point of the spray located around 10 mm from the nozzle tip. In addition, the spray begins to converge at around 7.5 mm. This spray also has an estimated focusing of region at the 9-12 mm location. In Nozzle B, faint streaks can be observed in the section between the nozzle tip and the stream convergence point, indicating that the grooves initially isolate the powder streams before convergence. These streaks are more prominently shown in Nozzle C, where they are more visible near the nozzle tip and converge at around the 9 mm point. The narrowest region of the powder stream is at around 15 mm, while the focusing region is estimated to be between 11.5 mm and 18 mm from the nozzle tip. As predicted in the simulations, the longer focusing region and further away waist location is attributed to the decrease in nozzle angle.

Simulation results for each corresponding nozzle show good correlation with the spray shape for Nozzles B and C, with the thinnest locations of the spray located at around 10 mm and 15 mm, respectively. However, Nozzle A produces a more defined spray shape in testing compared to the powder streamlines and concentration map. This is likely because the experimental setup can only capture parts of the spray profile with higher powder concentrations, whereas simulations can track every particle simulated and show their trajectories. In addition, it can be seen that air from the nozzle kicks up deposited powders within the collection tray into the air, creating noise that could obscure evidence of single powders diverging from the stream.

Despite these differences, examination of the sprays does show that the Nozzles B and C provide improved powder focusing. Measurements of the spray widths, shown in Fig. 14, reveal that Nozzles B and C have a smaller minimum average spray width, with the average being 1.25 mm and 1.23 mm, respectively. Nozzle A, meanwhile, has an average spray width of 1.51 mm, meaning that there is more divergence in powder trajectories without nozzles with grooves. This reduction of the minimum spray width (about 17.218.5 %) while also examining the overall spray shape shows that the addition of grooves within nozzles improves powder focusing. In addition, a steeper nozzle angle provides a larger powder focusing region, which may allow for more flexibility in DLMD operation while also allowing for more compact nozzles.

6. Conclusions

In the present study, a total of 16 designs were analyzed through CFD analysis and Full Factorial DOE analysis. In addition, three designs were manufactured and tested empirically to validate the CFD simulations. Through the simulations, it was determined that collision of the particles from the inlets onto the nozzle inner wall resulted in particles spreading throughout the nozzle. Although the gas flow and nozzle walls are able to direct the particles towards the nozzle exit, a typical continuous coaxial DLMD nozzle is unable to fully focus these powders as they are allowed to have a circumferential velocity component to their trajectory. This results in some powders not completely converging with the rest of the powder stream, effectively widening the powder spray area

and potentially reducing powder deposition efficiency. Important results from these tests include the following: • By using a flow-straightening geometry feature such as internal grooves, the circumferential velocity component is greatly minimized, improving powder focusing and reducing spray width at the focal point. CFD Simulations show that straight grooves of uniform width provide high powder concentration ($0.25–0.45\ kg/m^3$) at low inlet pressures ($1\ kPa$), and correspondingly have narrow powder cloud diameters ($6-8\ mm$). This effect does not change drastically with a change in nozzle angle. • Instead, the only important characteristics that are affected is the powder focal point location and ideal focus region. A 17° nozzle angle with grooves will have a powder focal point at 10 mm from the nozzle tip, whereas a 12° nozzle angle with grooves will have a powder focal point at 15 mm. The corresponding ideal focus regions are 9-12 mm for the 17° nozzle, and 11.5–18.5 mm for the 12° nozzle, meaning that a steeper nozzle angle will provide more room for error in standoff distances. • Empirical observation of the powder spray profiles confirmed the effectiveness of flow-straightening grooves in improving powder focusing, with grooved nozzles reducing average spray widths by around 0.25 mm compared to the control nozzle. This improved focusing comes at the cost of increasing powder velocity, with maximum powder velocities reaching up to 40 m/s at high inlet pressures. This increase velocity could result in powders rebounding off the melt pool or splashing into the melt pool. As such, inlet pressure or inlet gas flow rate must be controlled to ensure high powder catchment efficiency.

Despite the evidence, this work can further be improved by integrating them into a full DLMD system, laser included. This will allow the authors to create deposition samples that can be analyzed and compared with each other. Obtaining deposition results will help determine the spraying resolution: thickness, depth into the material, and height and deposition quality of each nozzle, allowing for a better understanding of how geometry features that improve powder focusing affects the overall DLMD process. In addition, this work can be integrated into models that incorporate CFD analysis into simulating powder-laser beam interactions to help determine how to optimize parameters such as powder feed rate and laser beam power.

Declaration of competing interest

The authors declare that they have no known competing financial interests or personal relationships that could have appeared to influence the work reported in this paper.

References

[1] Thompson SM, Bian L, Shamsaei N, Yadollahi A. An overview of direct laser deposition for additive manufacturing; part i: transport phenomena, modeling and diagnostics. Addit Manuf 2015;8:36–62. https://doi.org/10.1016/j.addma.2015.07.001.

[2] Masaylo D, Igoshin S, Popovich A, Popovich V. Effect of process parameters on defects in large scale components manufactured by direct laser deposition. Materials Today: Proceedings 2020;30:665–71. https://doi.org/10.1016/J.MATPR.2020.01.519.

[3] Francis J, Sparks TE, Ruan J, Liou F. Multi-axis tool path generation for surface finish machining of a rapid manufacturing process. Int J Rapid Manuf 2014;4:66. https://doi.org/10.1504/IJRAPIDM.2014.062040.

[4] Rosa B, Mognol P, Hascöet JYves. Laser polishing of additive laser manufacturing surfaces. Journal of Laser Applications 2015;27:S29102. https://doi.org/10.2351/1.4906385.

[5] Kerbrat O, Mognol P, Hascöet JY. A new dfm approach to combine machining and additive manufacturing. Computers in Industry 2011;62:684–92. https://doi.org/10.1016/J.COMPIND.2011.04.003.

[6] Kumar SP, Elangovan S, Mohanraj R, Srihari B. Critical review of off-axial nozzle and coaxial nozzle for powder metal deposition. Materials Today: Proceedings 2021. https://doi.org/10.1016/j.matpr.2021.03.037. 3.

[7] Williamson R. Method and system for producing speech signals. 2000. https://patents.google.com/patent/US6046426A/en.

[8] Li Y, Yang H, Lin X, Huang W, Li J, Zhou Y. The influences of processing parameters on forming characterizations during laser rapid forming. Mater Sci Eng A 2003;360:18–25. https://doi.org/10.1016/S0921-5093(03)00435-0.

[9] Silva MDD, Partes K, Seefeld T, Vollertsen F. Comparison of coaxial and off-axis nozzle configurations in one step process laser cladding on aluminum substrate. J Mater Process Technol 2012;212:2514–9. https://doi.org/10.1016/j.jmatprotec.2012.06.011.

[10] Zhong C, Pirch N, Gasser A, Poprawe R, Schleifenbaum JH. The influence of the powder stream on high-deposition-rate laser metal deposition with inconel 718. Metals 2017;7:443. https://doi.org/10.3390/met7100443.

[11] Arrizubieta JL, Tabernero I, Ruiz JE, Lamikiz A, Martinez S, Ukar E. Continuous coaxial nozzle design for lmd based on numerical simulation. Phys Procedia 2014;56:429–38. https://doi.org/10.1016/j.phpro.2014.08.146.

[12] Gabor TT, Joe HE, Akin S, Jun MBG, Kim KH, Park JK. Numerical investigation of various coaxial nozzle designs for direct laser deposition2; 2020. https://doi.org/10.1115/MSEC2020-8444.

[13] Tabernero I, Lamikiz A, Ukar E, Lacalle LNLD, Angulo C, Urbikain G. Numerical simulation and experimental validation of powder flux distribution in coaxial laser cladding. J Mater Process Technol 2010;210:2125–34. https://doi.org/10.1016/j.jmatprotec.2010.07.036.

[14] Xia Y, Huang Z, Chen H, Liang X, Lei J. Numerical simulation and experimental investigation on powder transport of a new-type annular coaxial nozzle. Int J Adv Manuf Technol 2021. https://doi.org/10.1007/s00170-021-07294-x.

[15] Lin J. Numerical simulation of the focused powder streams in coaxial laser cladding. J Mater Process Technol 2000;105:17–23. https://doi.org/10.1016/S0924-0136(00)00584-7.

[16] Wen SY, Shin YC, Murthy JY, Sojka PE. Modeling of coaxial powder flow for the laser direct deposition process. Int J Heat Mass Transf 2009;52:5867–77. https://doi.org/10.1016/j.ijheatmasstransfer.2009.07.018.

[17] Yang N. Concentration model based on movement model of powder flow in coaxial laser cladding. Opt Laser Technol 2009;41:94–8. https://doi.org/10.1016/J.OPTLASTEC.2008.03.008.

[18] Neto OOD, Alcalde AM, Vilar R. Interaction of a focused laser beam and a coaxial powder jet in laser surface processing. J Laser Appl 2007;19:84. https://doi.org/10.2351/1.2402523.

[19] Kovalev OB, Zaitsev AV, Novichenko D, Smurov I. Theoretical and experimental investigation of gas flows, powder transport and heating in coaxial laser direct metal deposition (dmd) process. 2011. https://doi.org/10.1007/s11666-010-9539-3.

[20] Liu H, He XL, Yu G, Wang ZB, Li SX, Zheng CY, Ning WJ. Numerical simulation of powder transport behavior in laser cladding with coaxial powder feeding. Sci China Phys Mech Astron 2015;58:104701. https://doi.org/10.1007/s11433-015-5705-4.

[21] Ibarra-Medina J, Pinkerton AJ. In: A cfd model of the laser, coaxial powder stream and substrate interaction in laser cladding. 5. Elsevier; 2010. p. 337–46. https://doi.org/10.1016/j.phpro.2010.08.060.

[22] Zhang J, Yang L, Zhang W, Qiu J, Xiao H, Liu Y. Numerical simulation and experimental study for aerodynamic characteristics and powder transport behavior of novel nozzle. Opt Lasers Eng 2020;126:105873. https://doi.org/10.1016/j.optlaseng.2019.105873.

[23] Zhang J, Yang L, Li Z, Zhang Q, Yu M, Fang C, Xiao H. Transport phenomenon, flow field, and deposition forming of metal powder in the laser direct deposition with designed nozzle. Int J Adv Manuf Technol 2021;114:1373–83. https://doi.org/10.1007/s00170-021-06913-x.

[24] N. Sobhanieh J. Akbari M. Moradi n.d. A new method for calculating laser intensity distribution on workpiece surface in laser-directed energy deposition process by considering powder stream distribution and laser attenuation, Int J Adv Manuf Technol 1 3. 10.1007/s00170-022-09301-1.

[25] Moradi M, Hasani A, Pourmand Z, Lawrence J. Direct laser metal deposition additive manufacturing of inconel 718 superalloy: statistical modelling and optimization by design of experiments. Optics and Laser Technology 2021;144. https://doi.org/10.1016/J.OPTLASTEC.2021.107380. 12.

[26] Nankali M, Akbari J, Moradi M, Beiranvand ZM. Effect of laser additive manufacturing parameters on hardness and geometry of inconel 625 parts manufactured by direct laser metal deposition. Optik 2022;249:168193. https://doi.org/10.1016/J.IJLEO.2021.168193.

[27] Guide FT. Ansys Fluent Theory Guide. 2013.

[28] Launder BE, Spalding BE, Brian D. Lectures in mathematical models of turbulence. new york: academic press; 1972.

[29] Morsi SA, Alexander AJ. An investigation of particle trajectories in two-phase flow systems. J Fluid Mech 1972;55:193–208. https://doi.org/10.1017/S0022112072001806.

[30] Hoppers/kegs. https://www.columbiacoatings.com/hoppers/kegs.aspx.